Electrochimica Acta 196 (2016) 611–621

Contents lists available at ScienceDirect

Electrochimica Acta

journal homepage: www.elsevier.com/locate/electacta

$NiCo_2O_4$@TiN Core-shell Electrodes through Conformal Atomic Layer Deposition for All-solid-state Supercapacitors

Ruiqi Wang[a,b], Chuan Xia[a], Nini Wei[a], Husam N. Alshareef[a,*]

[a] Materials Science and Engineering Department, King Abdullah University of Science and Technology (KAUST), Thuwal 23955-6900, Saudi Arabia
[b] The KAUST School, King Abdullah University of Science and Technology (KAUST), Thuwal 23955-6900, Saudi Arabia

ARTICLE INFO

Article history:
Received 26 January 2016
Received in revised form 1 March 2016
Accepted 3 March 2016
Available online 12 March 2016

Keywords:
Titanium nitride (TiN)
Core–shell
Atomic layer deposition (ALD)
All-solid-state
Supercapacitor

ABSTRACT

Ternary transition metal oxides such as $NiCo_2O_4$ show great potential as supercapacitor electrode materials. However, the unsatisfactory rate performance of $NiCo_2O_4$ may prove to be a major hurdle to its commercial usage. Herein, we report the development of $NiCo_2O_4$@TiN core–shell nanostructures for all-solid-state supercapacitors with significantly enhanced rate capability. We demonstrate that a thin layer of TiN conformally grown by atomic layer deposition (ALD) on $NiCo_2O_4$ nanofiber arrays plays a key role in improving their electrical conductivity, mechanical stability, and rate performance. Fabricated using the hybrid $NiCo_2O_4$@TiN electrodes, the symmetric all-solid-state supercapacitor exhibited an impressive stack power density of 58.205 mW cm^{-3} at a stack energy density of 0.061 mWh cm^{-3}. To the best of our knowledge, these values are the highest of any $NiCo_2O_4$-based all-solid-state supercapacitor reported. Additionally, the resulting $NiCo_2O_4$@TiN all-solid-state device displayed outstanding cycling stability by retaining 70% of its original capacitance after 20,000 cycles at a high current density of 10 mA cm^{-2}. These results illustrate the promise of ALD-assisted hybrid $NiCo_2O_4$@TiN electrodes within sustainable and integrated energy storage applications.

1. Introduction

As the technological development and widespread commercialization of increasingly demanding consumer electronics accelerate, the need for higher-performing energy storage systems grows faster than ever [1–4]. Throughout recent times, batteries have been widely regarded and employed as the most dominant energy storage device. But despite their ubiquity, affordability, and high energy density, batteries suffer from severe shortcomings such as high maintenance costs, low power density, and short cycling life [5].

Supercapacitors, on the other hand, have recently emerged as another promising energy storage device, showing great potential with their low maintenance needs, superior power density, and long cycle life. However, their relatively low energy density renders them ineffective in many practical applications [6]. Hence, the development of high-performance supercapacitors with increased energy and power capacities as well as extended cycling stability has been identified as a principal area of focus by commercial and research institutions alike [5,7–11]. Based on their energy storage mechanisms, supercapacitors can generally be classified into two categories: electrical double-layer capacitors (EDLCs) and pseudocapacitors. Carbonaceous materials are often employed in EDLCs to deliver double-layer capacitance through the accumulation of electrostatic charge on the carbon-based electrodes [8,12–16], while redox-active materials are commonly used in pseudocapacitors to store energy via fast and reversible surface redox reactions [17–22]. The growing interest in the latter, which includes conducting polymers and transition metal oxides/hydroxides, is driven by the vastly superior specific capacitance generated by the efficient Faradaic reactions in pseudocapacitors [23–26].

Due to their known redox activity and natural abundance, binary transition metal oxides (TMOs) such as NiO [27,28], TiO_2 [29], MnO_2 [30,31], Fe_2O_3 [32], and Co_3O_4 [31,33,34] have been extensively studied as electrode materials for pseudocapacitors [35]. More recently, ternary nickel cobaltite ($NiCo_2O_4$) has attracted considerable research attention due to its low cost, environmental friendliness, and high theoretical capacitance [36–40]. By having access to contributions from both nickel and cobalt ions, ternary $NiCo_2O_4$ also exhibits higher electrochemical activity, richer redox reactions, and significantly better electrical conductivity (over two orders of magnitude greater) compared to its corresponding binary oxides NiO and Co_3O_4 [24,35,41–43]. However, despite possessing a relatively greater conductivity than

* Corresponding author.
E-mail address: husam.alshareef@kaust.edu.sa (H.N. Alshareef).

http://dx.doi.org/10.1016/j.electacta.2016.03.015
0013-4686/

its binary counterparts, ternary $NiCo_2O_4$ still suffers from limited rate performance [44,45]. In order to improve the rate capability of $NiCo_2O_4$ electrodes, we introduced titanium nitride (TiN) to form $NiCo_2O_4$@TiN core-shell nanostructures with $NiCo_2O_4$. TiN attracted our attention due to the following reasons: 1) TiN is already commonly used in industry for electronics and wear resistance applications due to its low cost, scalability, and superior corrosion resistance [46,47]; 2) as a metallic material, TiN offers superb electrical conductivity (4000–55500 S cm^{-1}) and mechanical stability [48–50]; 3) previous reports have demonstrated that transition metal nitrides are capable of delivering high energy and power density as supercapacitor electrodes [51,52]. Meanwhile, by employing atomic layer deposition (ALD), we were able to conformally grow a TiN shell onto complex nanostructures such as the $NiCo_2O_4$ nanofiber arrays without altering the desired structural features of the underlying $NiCo_2O_4$ matrix.

While atomic layer deposited TiN coatings have been studied and employed in various lithium-ion battery applications [53–56], there has been little to no research on their potential in the context of supercapacitors. Herein, we report a novel strategy to synthesize nanostructured $NiCo_2O_4$@TiN core–shell nanofiber arrays for high-performance supercapacitors with significantly improved rate capability and electrochemical performance. Grown through ALD, the conformal ultrathin TiN coating not only acts as a mechanical buffering layer to help prevent the structural deformation of the underlying $NiCo_2O_4$ nanofiber arrays during repeated charge-discharge cycling, but also facilitates the transportation of electrons at the electrode/electrolyte interface. Additionally, the TiN shell contributes pseudocapacitively through Faradaic reactions at its oxidized surface layer [57]. By taking advantage of the combined electrochemical activity and mechanical stability of the ALD-assisted core–shell nanostructure, our symmetrical $NiCo_2O_4$@TiN all-solid-state supercapacitor exhibits an excellent stack power density (based on the thickness of the entire device) of 58.205 mW cm^{-3} at a high stack energy density of 0.061 mWh cm^{-3}, as well as outstanding cycling stability (~70% retention after 20,000 cycles at 10 mA cm^{-2}).

2. Experimental section

2.1. Preparation of $NiCo_2O_4$ Nanofiber Arrays

Chemicals of analytical grade were purchased from Sigma-Aldrich and used as received without further purification. $NiCo_2O_4$ nanofiber arrays were synthesized on carbon fiber cloth (CFC) substrate through a facile hydrothermal method. Typically, 2 mmol of $Ni(NO_3)_2{\cdot}6H_2O$, 4 mmol of $Co(NO_3)_2{\cdot}6H_2O$, and 7.5 mmol of urea were dissolved in 40 mL of DI water and left to stir on a magnetic stirrer for 10 minutes in air. The carbon fiber cloth substrate was then immersed in the bimetallic precursor solution before being transferred into a Yamato DNF-410Constant Temperature Oven. Next, the autoclave was heated to 120 °C for 4 hours and left to cool to room temperature naturally. After the precursor substrate was removed from the solution, it was cleaned through ultrasonification to remove loosely attached particles on the surface as well as washed with distilled water and methanol. The loaded substrate was then dried before being annealed in air at 350 °C for 2 h with a heating rate of 3 °C min^{-1}, converting the bimetallic carbonate hydroxide precursor into the desired $NiCo_2O_4$ nanofiber arrays.

2.2. Atomic Layer Deposition of TiN

Atomic layer deposition of TiN was carried out on an Oxford Instrument FlexAL Atomic Layer Deposition System, which offers both thermal and remote plasma ALD configurations. A commercially available liquid $TiCl_4$ precursor was contained in a canister at room temperature and subsequently nitridized by NH_3 plasma in the reaction chamber. Typically, an ALD cycle of TiN followed standard deposition process according to the following sequence: a 0.1 s pulse of $TiCl_4$ vapor, a 3 s purge by Ar gas, a 7 s pulse of NH_3 plasma, and another 3 s purge by Ar gas. The temperature was maintained at 350 °C throughout all 300 ALD cycles.

2.3. Materials Characterization

The structures and morphologies of samples were characterized by SEM (Nova Nano 630, FEI) and TEM (Titan 80–300 kV (ST) TEM, FEI). The phase purity of samples were examined through powder XRD (Bruzer D8 Advance).

2.4. Electrochemical Measurements

Electrochemical tests were conducted on a VMP3 multichannel electrochemical workstation (Bio-Logic) in both three-electrode (half-cell) and two-electrode (full-cell) configurations. In three-electrode measurements, $NiCo_2O_4$ or $NiCo_2O_4$@TiN coated carbon cloth was employed as the working electrode, a Pt wire as the counter electrode, and Ag|AgCl as the reference electrode. All three-electrode measurements were carried out within a voltage window of −0.1 V to 0.6 V in 1 M KOH aqueous electrolyte solution.

For two-electrode configurations, symmetrical aqueous coin cells and all-solid-state devices were assembled. Aqueous coin cells were fabricated by sandwiching a separator (Celgard 3501) between two identical $NiCo_2O_4$ or $NiCo_2O_4$@TiN electrodes. Several drops of 1 M KOH aqueous electrolyte were added before the components were sealed in a CR2032 stainless-steel coin cell. Symmetrical all-solid-state devices were assembled by sandwiching a layer of PVA/KOH gel electrolyte between two identical $NiCo_2O_4$@TiN electrodes. All two-electrode measurements were conducted within a voltage window of 0 V to 0.8 V.

All single electrodes and full-cell devices were evaluated using cyclic voltammetry (CV), galvanostatic charge-discharge (CD), and electrochemical impedance spectroscopy (EIS) at room temperature. The absolute capacitance (in F) was derived from CV curves or CD curves according to the following equations

$$C = \frac{i}{v_{scan}}$$

$$C = \frac{I}{\frac{\Delta V}{\Delta t}}$$

where i is the average cathodic current of the CV curve, v_{scan} is the scan rate, I is the constant current of charge-discharge and $\frac{\Delta V}{\Delta t}$ is the slope of the discharge curve, excluding the IR drop. The areal capacitance and cell capacitance (in F cm^{-2}) were then calculated through

$$C_{areal} = \frac{C}{A_{elec}}$$

$$C_{cell} = \frac{C}{A_{overlap}}$$

where A_{elec} is the area of the electrode in three-electrode configuration, and $A_{overlap}$ is the overlapping area of the two electrodes of a full cell in two-electrode configuration.

In order to effectively evaluate the electrochemical performance of the full supercapacitor device, the key parameters stack energy density (E) and power density (P) were calculated based on

the following equations

$$E = \frac{1}{2}C_{cell}V^2$$

$$P = \frac{E}{\Delta t} = \frac{\frac{1}{2}C_{cell}V^2}{\Delta t}$$

where C_{cell} is the cell capacitance derived above, V is the voltage window applied during the charge-discharge measurements, and Δt is the discharge time obtained from CD curves.

3. Results and discussion

The $NiCo_2O_4$@TiN core-shell nanofiber arrays were prepared through a facile two-step approach. First, nanostructured $NiCo_2O_4$ was grown hydrothermally on CFC substrate as outlined in the experimental section. Next, an ultrathin layer of TiN was controllably deposited over 300 ALD cycles to form a highly conductive hybrid electrode. ALD is a thin film growth technique that allows for the uniform deposition of conformal ultrathin films [58] on high-aspect-ratio substrates [59,60] or nanoparticles [26,61]. Scanning electron microscopy (SEM) images of the $NiCo_2O_4$ nanostructures before the ALD of TiN are shown in Fig. 1a,b. Evidently, the as-synthesized $NiCo_2O_4$ nanofiber arrays achieved high specific area and uniform coverage of the CFC substrate. After 300 ALD cycles of TiN, we conducted X-ray diffraction (XRD) analysis to examine the phase purity of the product, as displayed in Fig. 1**c**. The clearly identifiable peaks of spinel $NiCo_2O_4$ (JCPDS No. 02-1074) indicate that the spinel structure of the underlying $NiCo_2O_4$ arrays was well-preserved underneath the ultrathin TiN shell. The remaining peaks can be readily indexed to CFC and cubic TiN (JCPDS No. 38-1420). No unidentified diffraction peaks from possible impurities are detected, demonstrating the successful growth of $NiCo_2O_4$@TiN core-shell nanofiber arrays and the high purity of the product. Fig. 1d–f show the morphology and structural properties of $NiCo_2O_4$@TiN composite after 300 ALD cycles of TiN at low and high magnifications. Owing to the conformal nature of the ALD technique, the $NiCo_2O_4$@TiN core–shell nanostructures retained the large surface area of the pristine $NiCo_2O_4$ arrays, which is highly desirable in energy storage applications.

Transmission electron microscopy (TEM) characterization was carried out to further investigate the core-shell structure of the as-prepared $NiCo_2O_4$@TiN arrays. Fig. 2a reveals the porous nature of pure $NiCo_2O_4$ nanofibers. Upon closer examination of Fig. 2b, the rough surface and mesopores (with diameters of ~4 nm) can be clearly identified. It is well-established that mesoporous structures increase the specific area and number of accessible active sites of the material, allowing for improved electrode/electrolyte contact and enhanced charge storage capacity. Additionally, the mesopores act as effective transportation channels that help facilitate the mass transport of electrolyte ions within the electroactive materials for rapid redox reactions and charge adsorption on the electrode surface. The smooth outer shell of TiN surrounding the grainlike $NiCo_2O_4$ nanofiber core, as displayed in Fig. 2c,d, shows that the thin coating of TiN (with thickness of ~8 nm) has indeed been conformally deposited over the underlying $NiCo_2O_4$ matrix. While precise, ALD does result in some characteristic pinholes and discontinuities, which have been observed in a previous study on ALD-grown PANI@RuO_2 core-shell structures as well [26]. These ALD pinholes, as observed in Fig. S1 (Supporting Information), serve as pathways for the electrolyte to make contact and react with the otherwise covered $NiCo_2O_4$. The high-resolution transmission electron microscopy (HRTEM) shown in Fig. 2e reveals lattice fringes (with spacing of 0.287 nm) that can be readily indexed to the (220) plane of spinel $NiCo_2O_4$ phase. Similarly, the outer TiN shell is observed to have an interplanar

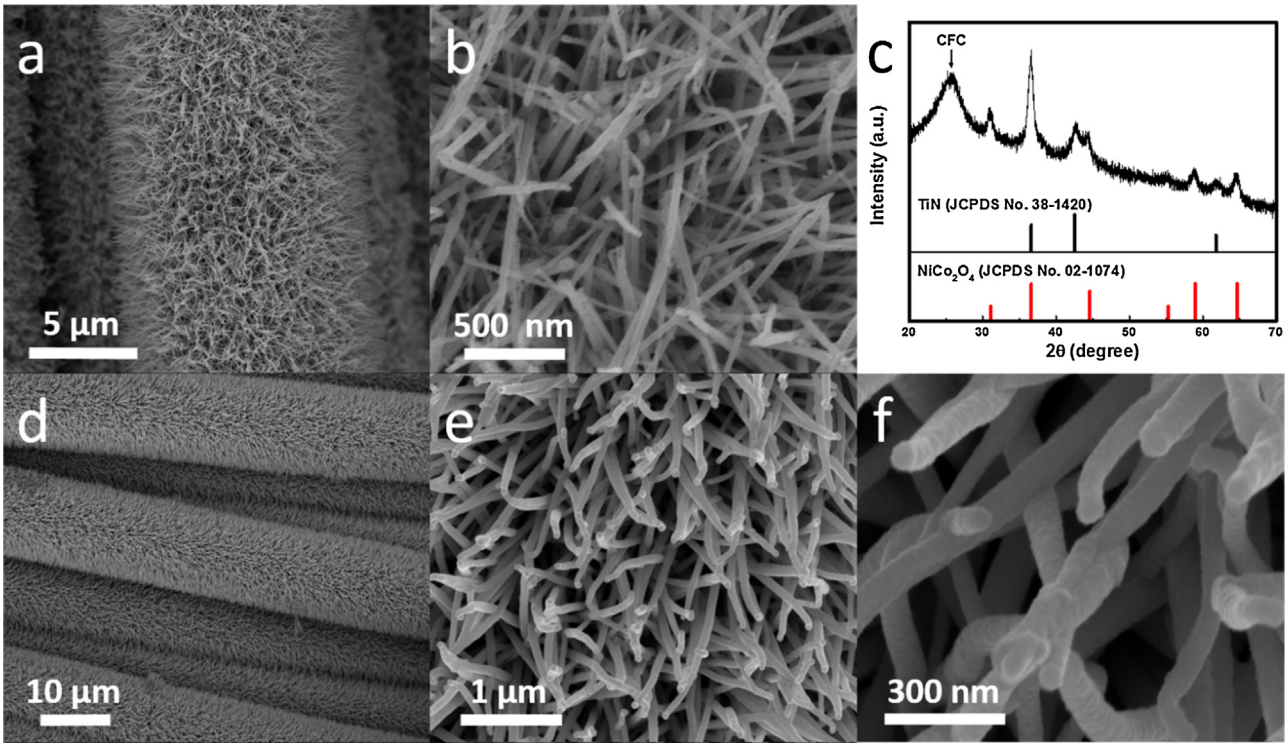

Fig. 1. (a,b) SEM images of $NiCo_2O_4$. (c) XRD pattern of $NiCo_2O_4$@TiN core-shell nanofiber arrays supported on carbon fiber cloth. (d–f) SEM images of $NiCo_2O_4$@TiN.

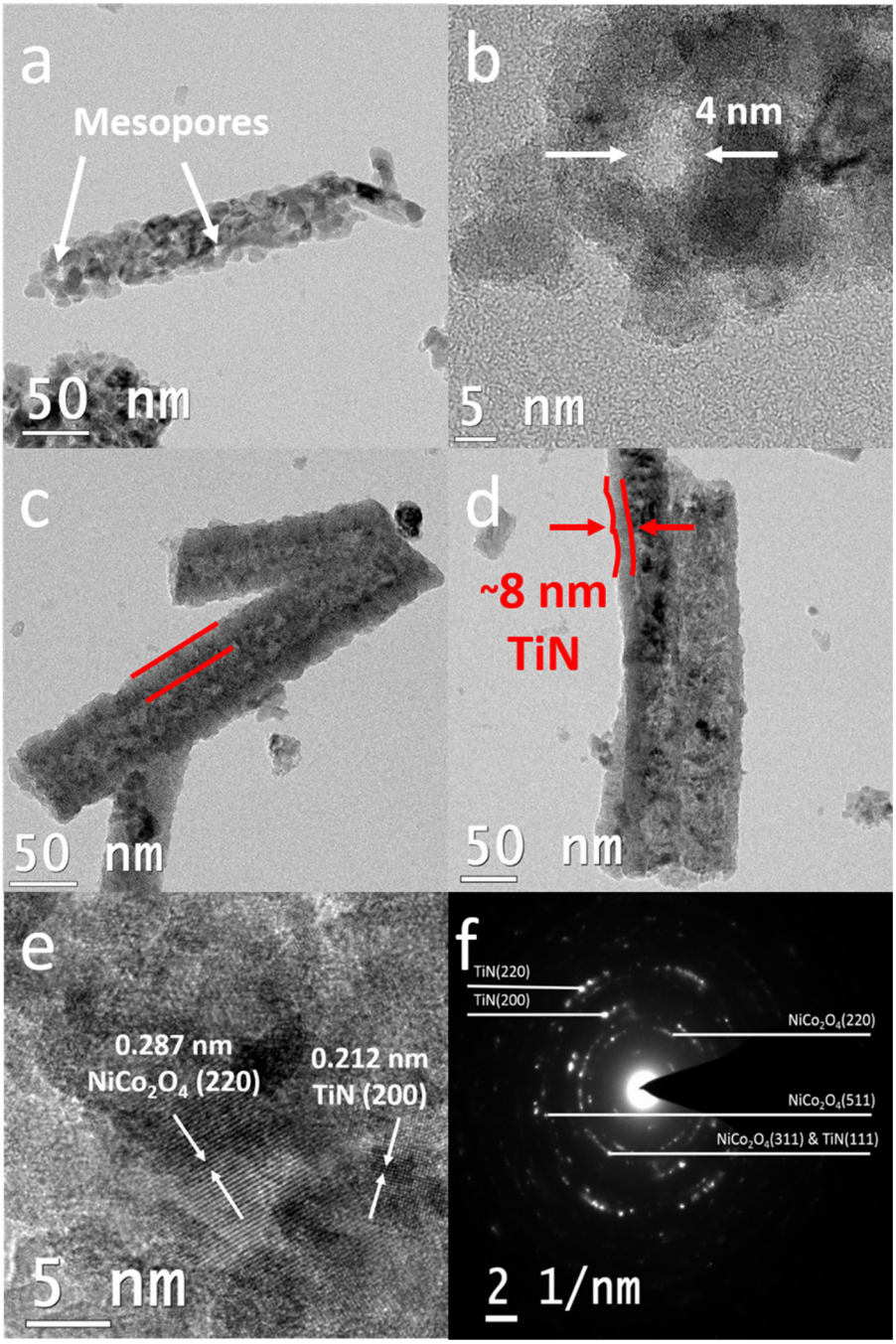

Fig. 2. TEM images of (a,b) $NiCo_2O_4$ and (c–e) $NiCo_2O_4$@TiN. (f) SAED pattern showing (220), (311), and (511) lattice planes of $NiCo_2O_4$ as well as (111), (200), and (220) lattice planes of TiN.

spacing of 0.212 nm, which corresponds to the (200) plane of TiN. The polycrystalline nature of the materials is further confirmed by the selected area electron diffraction (SAED) pattern as depicted in Fig. 2f, in which a series of diffraction rings can be readily assigned to the (220), (311), and (511) planes of the cubic $NiCo_2O_4$ phase and the (111), (200), and (220) planes of the cubic TiN phase.

To evaluate the electrochemical performances of pure $NiCo_2O_4$ and $NiCo_2O_4$@TiN nanofiber arrays supported on CFC substrate, cyclic voltammetry (CV) measurements of $NiCo_2O_4$ and $NiCo_2O_4$@-TiN individual electrodes were carried out at different scan rates, as shown in Fig. 3a,b respectively. The redox peaks present in the CV curves of both electrodes demonstrate typical pseudocapacitive behavior. In Fig. 3a, a pair of redox peaks at 0.28 V and 0.45 V are observed for the bare $NiCo_2O_4$ nanofiber arrays at a scan rate of 5 mV s^{-1}, which are assigned to the reversible redox reactions of Ni^{2+}/Ni^{3+} and $Co^{2+}/Co^{3+}/Co^{4+}$ transitions associated with OH^- anions. In Fig. 3b, a pair of redox peaks at 0.24 V and 0.44 V are observed for the $NiCo_2O_4$@TiN core-shell nanofiber arrays at the same scan rate of 5 mV s^{-1}. The change in the positions of the redox peaks may be attributed to the pseudocapacitive contributions of the TiN shell. As the scan rate increases, the hybrid $NiCo_2O_4$@TiN electrode appears to be much better at retaining the shape of its CV

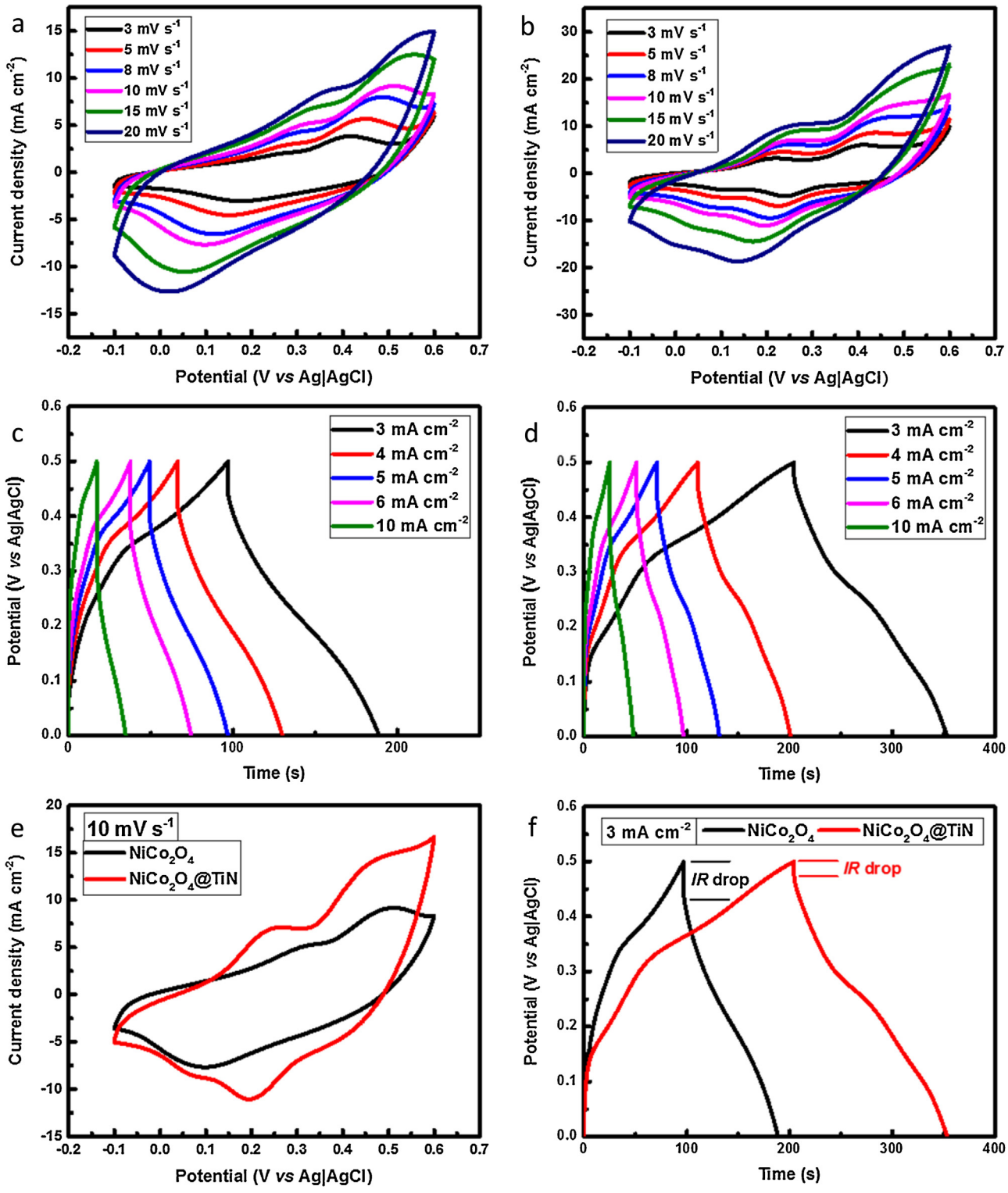

Fig. 3. Electrochemical evaluation of bare $NiCo_2O_4$ and hybrid $NiCo_2O_4$@TiN individual electrodes in aqueous electrolyte. CV curves of (a) $NiCo_2O_4$ and (b) $NiCo_2O_4$@TiN electrodes. CD curves of (c) $NiCo_2O_4$ and (d) $NiCo_2O_4$@TiN electrode. (e) Comparison of CV curves of $NiCo_2O_4$ and $NiCo_2O_4$@TiN electrodes at scan rate of 10 mV s^{-1}. (f) Comparison of CD curves of $NiCo_2O_4$ and $NiCo_2O_4$@TiN electrodes at current density of 3 mA cm^{-2}.

curve than the pristine $NiCo_2O_4$ electrode, suggesting that the rate performance of the hybrid electrode is vastly superior.

To further investigate the electrochemical properties of the electrodes, galvanostatic charge-discharge (CD) measurements were conducted at various current densities. The areal capacitances of the bare $NiCo_2O_4$ electrode were derived from the CD curves in Fig. 3c to be 670, 631, 602, 553, 384, and 281 mF cm^{-2} at current densities of 2, 3, 5, 10, 15, and 20 mA cm^{-2} respectively, as shown in Fig. S2a (Supporting Information), whereas those of the hybrid $NiCo_2O_4$@TiN electrode were calculated from the CD curves in Fig. 3d to be 998, 954, 714, 601, 586, and 582 mF cm^{-2} at current densities of 2, 3, 5, 10, 15, and 20 mA cm^{-2} respectively, as shown in Fig. S2b (Supporting Information). Given a tenfold increase in current density, the hybrid $NiCo_2O_4$@TiN electrode retained ~59%

of its initial capacitance, far surpassing the pristine $NiCo_2O_4$ electrode which only retained ~42%. Evidently, adding the outer TiN shell has significantly increased the areal capacitance and rate performance of the bare $NiCo_2O_4$ electrodes. Fig. 3e shows the CV curves of the bare $NiCo_2O_4$ and hybrid $NiCo_2O_4$@TiN electrodes at an identical scan rate of 10 mV s^{-1}. The positions of the redox peaks have shifted after the ALD of TiN, which can be attributed to the pseudocapacitive contributions of the outer TiN shell. In addition, the integrated area within the CV curve of the hybrid $NiCo_2O_4$@TiN electrode is substantially larger than that of the bare $NiCo_2O_4$ electrode, again indicating that adding the outer TiN shell has considerably increased the electrode's overall electrochemical activity. Fig. 3f depicts the CD curves of the pure $NiCo_2O_4$ and hybrid $NiCo_2O_4$@TiN electrodes at an identical current density of 3 mA cm^{-2}. Consistent with the findings of the CV curves, the discharge period of the $NiCo_2O_4$@TiN electrode is considerably

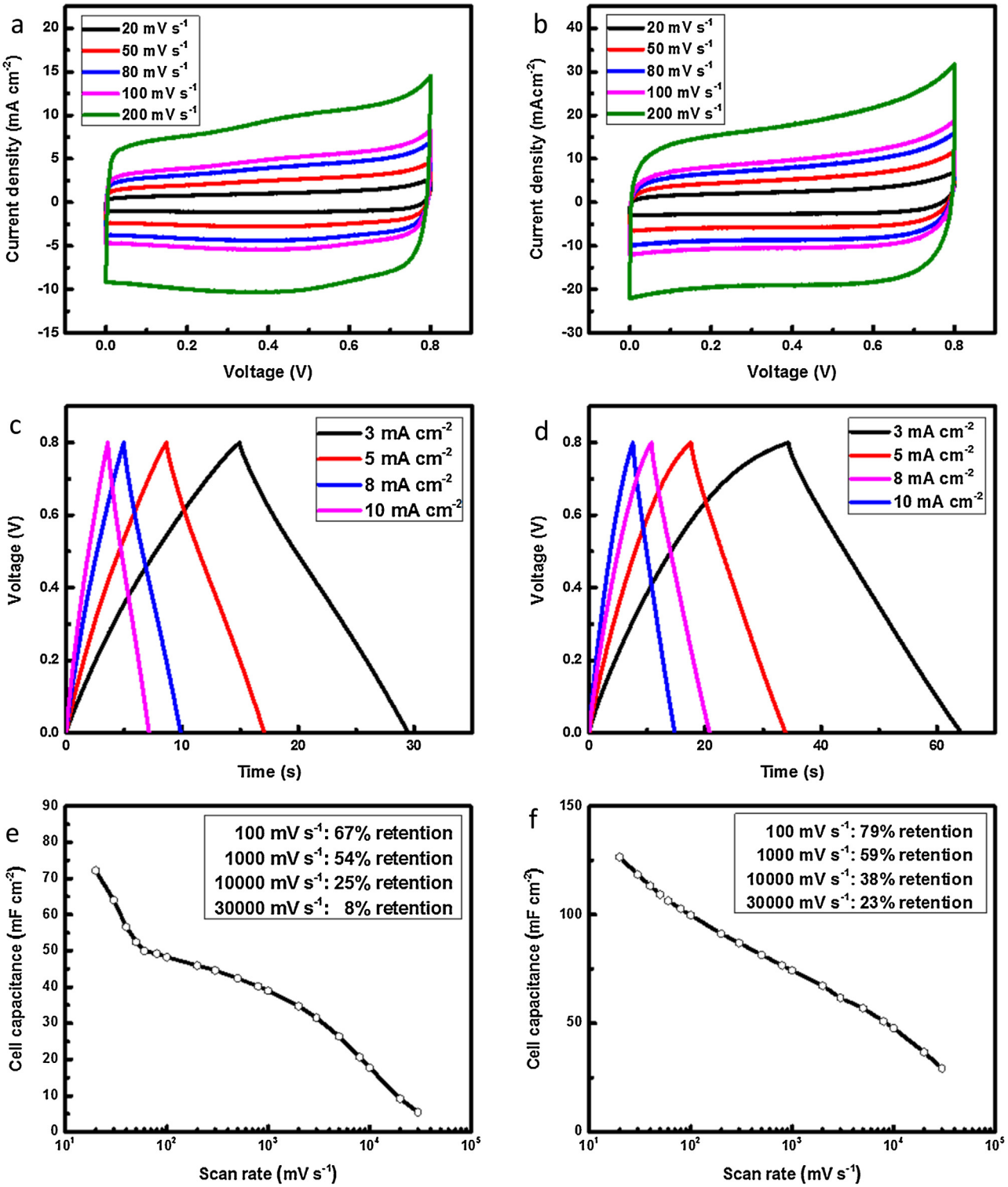

Fig. 4. Electrochemical evaluation of bare $NiCo_2O_4$ and core-shell $NiCo_2O_4$@TiN aqueous coin cells. CV curves of (a) $NiCo_2O_4$ and (b) $NiCo_2O_4$@TiN at various scan rates. CD curves of (c) $NiCo_2O_4$ and (d) $NiCo_2O_4$@TiN at various current densities. Capacitance retention of (e) $NiCo_2O_4$ and (f) $NiCo_2O_4$@TiN as a function of scan rate.

longer than that of the $NiCo_2O_4$ electrode. Furthermore, adding the outer TiN shell appears to have dramatically reduced the *IR* drop and internal resistance of the bare $NiCo_2O_4$ nanofiber array electrode. Consequently, the hybrid $NiCo_2O_4$@TiN electrode has been shown to surpass the pristine $NiCo_2O_4$ electrode in terms of electrical conductivity, areal capacitance, and overall electrochemical performance.

To further demonstrate the feasibility of $NiCo_2O_4$@TiN core-shell nanofiber arrays in practical energy storage applications, symmetrical full device prototypes of both $NiCo_2O_4$ and $NiCo_2O_4$@TiN were fabricated with 1 M KOH aqueous electrolyte for in-depth comparison. Fig. 4a,b illustrate the CV curves of $NiCo_2O_4$ and $NiCo_2O_4$@TiN aqueous devices at scan rates ranging from 20 mV s^{-1} to 200 mV s^{-1}. Notably, both pristine $NiCo_2O_4$ and core-shell $NiCo_2O_4$@TiN aqueous cells exhibited impressive rate capability by retaining the general shape of the quasi-rectangular curves from the scan rates of 20 mV s^{-1} to 200 mV s^{-1}. Based on the promising rate performance displayed thus far, we tested the assembled $NiCo_2O_4$ and $NiCo_2O_4$@TiN coin cells at even higher scan rates (up to an extremely high scan rate of 30,000 mV s^{-1}), as shown in Fig. S3a,b (Supporting Information) respectively. The pure $NiCo_2O_4$ aqueous cell managed to preserve its quasi-rectangular CV curve up to an impressive 5,000 mV s^{-1}, but lost its general shape beyond that point. Remarkably, on the other hand, the core-shell $NiCo_2O_4$@TiN aqueous cell retained its quasi-rectangular CV curve up to an extremely high scan rate of 20,000 mV s^{-1}, displaying immensely promising rate capability.

Next, the cell capacitances of both cells were derived from their CV curves and plotted against a wide range of scan rates, as depicted in Fig. 4c,d. At a scan rate of 100 mV s^{-1}, the pristine $NiCo_2O_4$ cell retained 67% of its initial cell capacitance, whereas the core-shell $NiCo_2O_4$@TiN cell exhibited a much higher rate capability of 79%. This substantial difference in rate performance becomes even more evident as the scan rate increases. At the extremely high scan rates of 10,000 mV s^{-1} and 30,000 mV s^{-1}, the pure $NiCo_2O_4$ cell retained 25% and 8% of its original cell capacitance, which were clearly surpassed by the excellent rate capabilities of 38% and 23% of the $NiCo_2O_4$@TiN cell. This considerable improvement in rate performance can be attributed to the metallic TiN shell being directly grown on the $NiCo_2O_4$ nanofiber arrays through ALD, resulting in the strong bonding and coupling between $NiCo_2O_4$ and TiN in the hybrid nanostructure. The above-mentioned results reveal the promise of the novel approach of enhancing an electrode's rate performance through the ALD of an outer TiN coating over another layer of active material to form a core-shell nanostructure. Additionally, the thickness of the outer TiN shell is tunable by controlling the number of ALD cycles, thus allowing for greater optimization and customizability to fit the electrochemical and structural properties of the underlying core material. Fig. 4e,f show the CD curves of the bare $NiCo_2O_4$ cell and the core-shell $NiCo_2O_4$@TiN cell respectively.

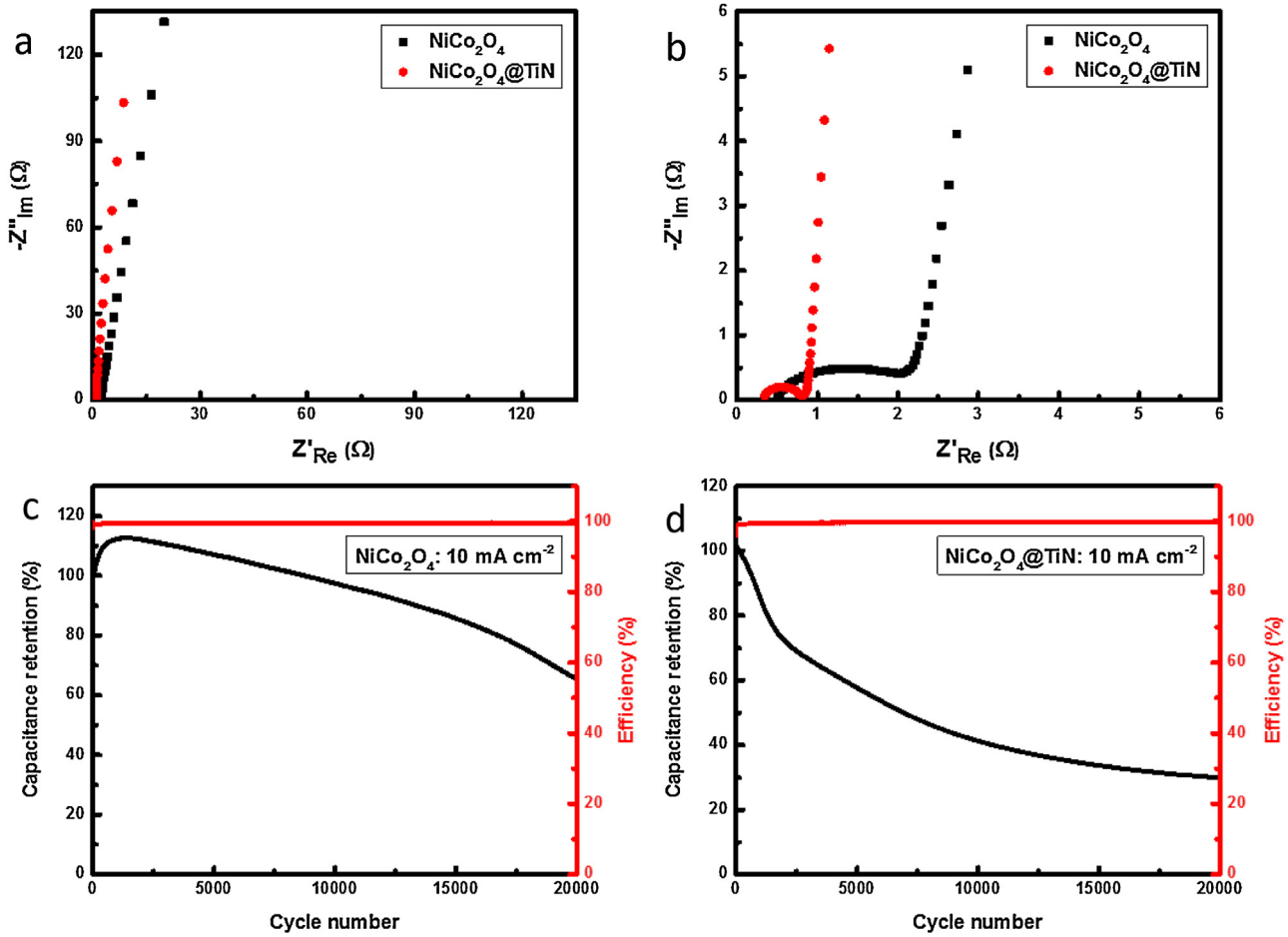

Fig. 5. (a,b) Nyquist plots of $NiCo_2O_4$ and $NiCo_2O_4$@TiN aqueous cells. Cycling performance of (c) $NiCo_2O_4$ and (d) $NiCo_2O_4$@TiN aqueous cells at a high current density of 10 mA cm^{-2} over 20,000 cycles.

Both cells displayed very symmetrical CD curves, indicating the high efficiency of the assembled devices. Even at relatively high current densities, such as 10 mA cm^{-2}, the *IR* drops observed are still very small for both cells, suggesting that they possess low equivalent series resistance (ESR) values.

Such low ESR values were further confirmed by the electrochemical impedance spectroscopy (EIS) measurements, as shown in Fig. 5a,b. Between the two aqueous cells, the smaller ESR value of the $NiCo_2O_4$@TiN cell (~0.34Ω) reflects the superior electrical conductivity of the integrated hybrid electrodes. From the diameters of the semicircles, the charge transfer resistance (R_{ct}) values of the pure $NiCo_2O_4$ and core-shell $NiCo_2O_4$@TiN coin cells were derived to be ~2.31Ω and ~0.46Ω respectively. Evidently, the charge transfer resistance has been dramatically reduced after 300 ALD cycles of TiN, again demonstrating how the deposition of a metallic TiN shell has significantly improved the electrical conductivity of the electrodes. The efficiency and cycling stability of the $NiCo_2O_4$ and $NiCo_2O_4$@TiN aqueous cells were evaluated at a high current density of 10 mA cm^{-2} over 20,000 cycles, as shown in Fig. 5c,d respectively. It is worth noting that both the pristine $NiCo_2O_4$ and core-shell $NiCo_2O_4$@TiN coin cells maintain a high efficiency of close to 100% throughout the cycling process. Additionally, the pure $NiCo_2O_4$ cell retained an impressive ~65.3% of its initial capacitance after 20,000 charge-discharge cycles. In contrast, the $NiCo_2O_4$@TiN cell suffered a sharp decrease in capacitance in the early stages, holding on to only ~72.2% of its original capacitance after just 2,000 cycles. Overall, the core-shell $NiCo_2O_4$@TiN cell retained only ~41.3% and ~29.9% of its initial capacitance after 10,000 and 20,000 charge-discharge cycles respectively. The poor cycling performance of the $NiCo_2O_4$@TiN cell is ascribed to the irreversible electrochemical oxidation and structural degradation of TiN in the aqueous electrolyte. Previous studies have found that in aqueous solution, TiN is quickly oxidized to form TiO_2, which is drastically less electrically conductive and electrochemically active [50]. Additionally, TiN may also suffer structural breakdown in the aqueous solution from repeated charge-discharging. Thus, the dramatic loss of capacitance that we observed can be assigned to the undesirable electrochemical oxidation and structural degradation of the ALD-grown outer TiN shell in aqueous electrolyte.

It is well-established that the key to improving the stability of TiN-based electrodes and devices is suppressing the irreversible electrochemical oxidation and structural breakdown [50]. Herein, we employ solid-state polymer electrolyte to enhance the electrochemical and structural stability of the outer TiN shell and consequently the entire $NiCo_2O_4$@TiN core-shell nanofiber arrays. By limiting the amount of water, solid-state polymer electrolyte can not only effectively subdue the electrochemical oxidation of TiN into TiO_2 [50], but also mechanically stabilize the TiN-coated $NiCo_2O_4$ nanofiber arrays by retaining their active sites and overall morphology during the cycling. Compared to cells using liquid-based electrolytes, all-solid-state devices also offer

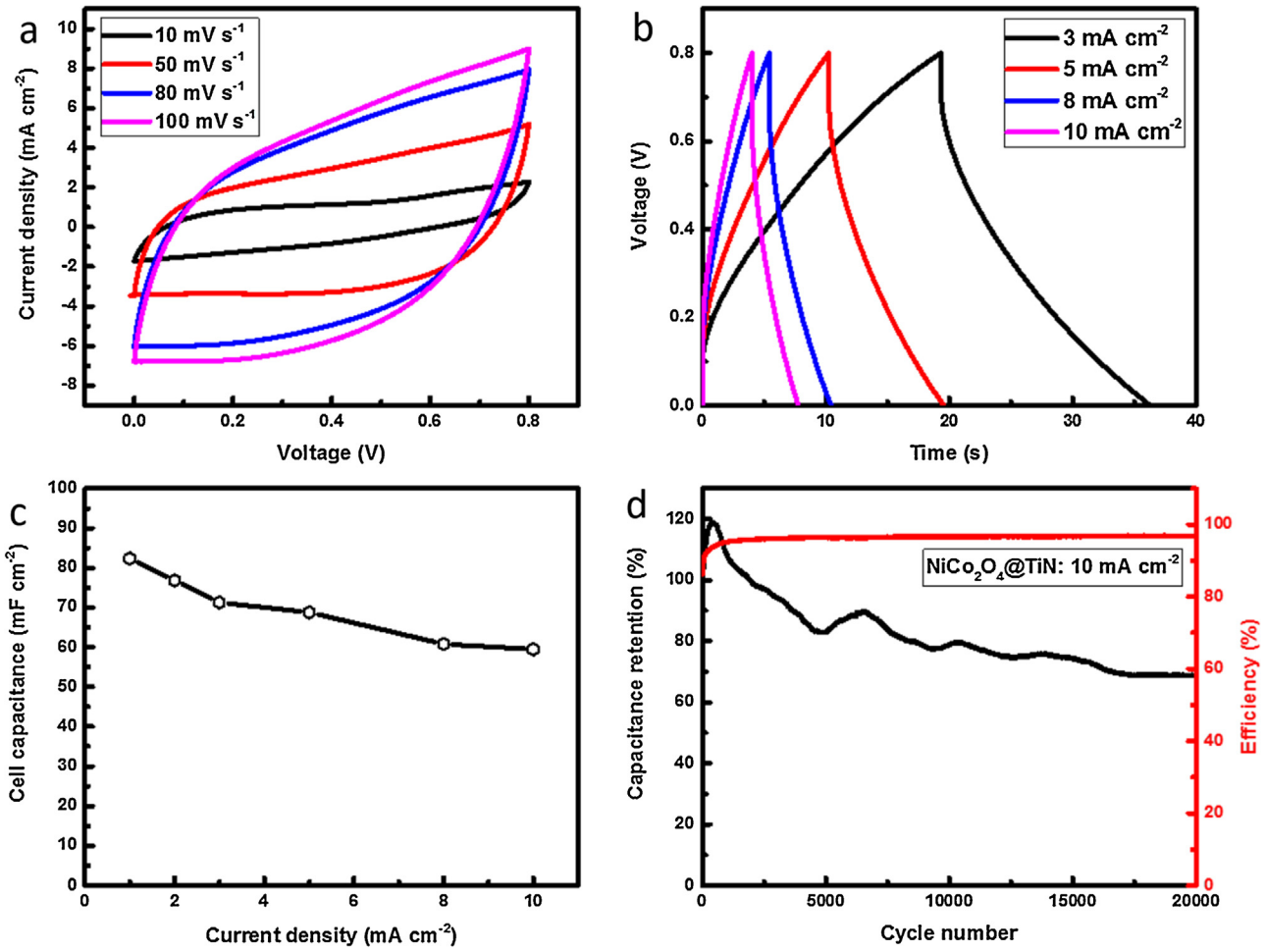

Fig. 6. Electrochemical evaluation of symmetrical $NiCo_2O_4$@TiN all-solid-state device. (a) CV curves at various scan rates ranging from 10 mV s^{-1} to 100 mV s^{-1}. (b) CD curves at various current densities ranging from 3 mA cm^{-2} to 10 mA cm^{-2}. (c) Cell capacitance as a function of current density. (d) Cycling performance at a high current density of 10 mA cm^{-2} over 20,000 cycles.

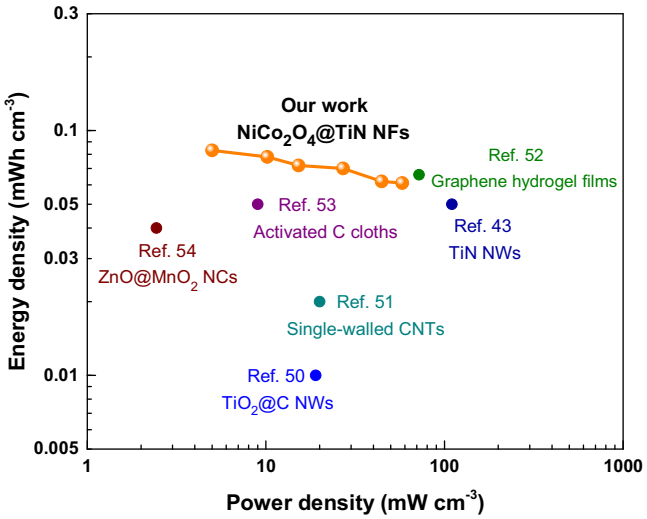

Fig. 7. Ragone plot of $NiCo_2O_4$@TiN all-solid-state supercapacitor in comparison with reported energy and power density values of other solid-state devices.

numerous practical advantages such as lighter weight, greater flexibility, increased reliability, improved safety, and wider operating temperate range [50], which are all highly desirable qualities in portable electronics and commercial energy storage applications.

As observed in Fig. 6a, the CV curves of the $NiCo_2O_4$@TiN all-solid-state device have assumed a quasi-rectangular shape similar to those of the aqueous coin cells evaluated above. The same trend is also evident in Fig. 6b, in which the CD curves are noticeably less symmetrical with visibly larger *IR* drops. As depicted in Fig. 6**c**, the cell capacitances of the $NiCo_2O_4$@TiN all-solid-state device were derived from the CD curves to be 82, 77, 71, 69, 61, and 60 mF cm^{-2} at the current densities of 1, 2, 3, 5, 8, and 10 mA cm^{-2}, which are comparably lower than those exhibited by the $NiCo_2O_4$@TiN aqueous cell. These changes in electrochemical behavior and properties can be attributed to the slightly less efficient mechanism of ion transport and diffusion in the polymer-based electrolyte.

Fortunately, these modest drawbacks are reasonably overshadowed by the significant improvement in cycling stability displayed in Fig. 6d. After 10,000 charge-discharge cycles at a high current density of 10 mA cm^{-2}, the $NiCo_2O_4$@TiN all-solid-state device retained ~78.9% of its initial capacitance, almost doubling the ~41.3% retained by the $NiCo_2O_4$@TiN aqueous cell. Notably, the rate of capacitance loss substantially slows down throughout the cycling process, to the extent where the $NiCo_2O_4$@TiN all-solid-state device maintained an exceptionally stable capacitance retention rate of ~70% over the last 2,500 cycles of the 20,000-cycle test. This excellent improvement in cycling stability is primarily attributed to the solid-state polymer electrolyte's suppression of the undesirable electrochemical oxidation and structural degradation of the TiN coating. Additionally, since the outer TiN shell is no longer limited by the issues associated with using aqueous electrolyte, it can also act as a mechanical buffering layer that helps to prevent the structural deformation of the underlying $NiCo_2O_4$ nanofiber arrays during repeated charge-discharge cycling. Furthermore, the conformal TiN shell is able to tolerate the volumetric swelling and shrinking, acting as a highly conductive network to hold together fragments of active materials and preserve their mechanical and electrochemical stability. This impressive cycling performance reveals the excellent potential of the $NiCo_2O_4$@TiN all-solid-state device in long-term industrial and durable commercial electronic applications.

As the two key parameters most directly relevant to the electrochemical performance of a full supercapacitor device in practical applications, the stack energy and power densities of the $NiCo_2O_4$@TiN all-solid-state device were derived and plotted in Fig. 7. The $NiCo_2O_4$@TiN all-solid-state device exhibited a maximum stack energy density of 0.083 mWh cm^{-3} at a stack power density of 5.005 mW cm^{-3}. Moreover, it is worth noting that as the stack power density increases from 5.005 mW cm^{-3} to 58.205 mW cm^{-3}, the stack energy density descends very gradually from 0.083 mWh cm^{-3} to 0.061 mWh cm^{-3}. These values are superior to those of previously reported solid-state devices, including supercapacitors based on TiO_2@C core-shell nanowires (0.01 mWh cm^{-3} at 19 mW cm^{-3}) [62], single-walled carbon nanotubes (0.02 mWh cm^{-3} at 20 mW cm^{-3}) [63], TiN nanowires (0.05 mWh cm^{-3} at 101 mW cm^{-3}) [50], 3D graphene hydrogel films (0.066 mWh cm^{-3} at 72 mW cm^{-3}) [64], activated carbon cloths (0.05 mWh cm^{-3} at 2 mW cm^{-3}) [65], and ZnO@MnO_2 core-shell nanocables (0.04 mWh cm^{-3} at 2.44 mW cm^{-3}) [66].

Achieving a high power density without largely sacrificing energy density indicates the significantly improved electrochemical performance of $NiCo_2O_4$@TiN nanofiber arrays, which can be attributed to their novel hybrid nanostructure. Additionally, the highly conductive $NiCo_2O_4$@TiN core-shell nanofiber arrays were directly grown on the CFC substrate, thus forming integrated electrodes with easily accessible pathways for the rapid transportation and diffusion of ions and electrons as well as greatly enhancing the charge transfer mechanism of the device. Furthermore, both the TiN shell and polymer gel electrolyte act as buffering layers that tolerate the electrochemical and structural degradation of the electrodes and preserve the energy density of the device even at high current densities, making the core-shell $NiCo_2O_4$@TiN all-solid-state supercapacitor a promising candidate for many increasingly demanding energy storage systems.

4. Conclusion

In summary, symmetrical all-solid-state supercapacitors were fabricated by growing $NiCo_2O_4$@TiN core-shell nanofiber arrays on carbon fiber cloth to form integrated high-performance electrodes.

In doing so, we have demonstrated for the first time that the conformal atomic layer deposition (ALD) of an ultrathin TiN shell onto a $NiCo_2O_4$ core can significantly enhance the rate capability and overall electrochemical performance of bare $NiCo_2O_4$ electrodes. Electrochemical measurements revealed that the $NiCo_2O_4$@TiN core-shell arrays maintained their strong electrochemical performance up to an extremely high scan rate of 20,000 mV s^{-1}, clearly outperforming the pure $NiCo_2O_4$ arrays in terms of areal capacitance and rate performance. Additionally, the symmetrical $NiCo_2O_4$@TiN all-solid-state device exhibited an excellent stack power density of 58.205 mW cm^{-3} at a high stack energy density of 0.061 mWh cm^{-3}, as well as outstanding cycling stability (~70% retention after 20,000 cycles at 10 mA cm^{-2}). Our work illustrates that conformally growing a TiN coating onto a $NiCo_2O_4$ matrix is a promising general approach that can be extended to other metal nitrides (VN, Fe_2N) and ternary metal oxides ($CuCo_2O_4$, $ZnFe_2O_4$) to fabricate enhanced high-performance supercapacitor devices for a wide range of sustainable and integrated energy storage applications.

Acknowledgements

The research reported in this publication has been supported by King Abdullah University of Science and Technology (KAUST). Ruiqi Wang thanks the KAUST Visiting Student Research Program for the excellent opportunity. The authors thank the staff of the KAUST Nanofabrication, Thin Film, Imaging, and Characterization Core Laboratories for their wonderful support.

Appendix A. Supplementary data

Supplementary data associated with this article can be found, in the online version, at http://dx.doi.org/10.1016/j.electacta.2016.03.015.

References

[1] M. Armand, J.-M. Tarascon, Building better batteries, Nature 451 (2008) 652–657.
[2] A.S. Arico, P. Bruce, B. Scrosati, J.-M. Tarascon, W. Van Schalkwijk, Nanostructured materials for advanced energy conversion and storage devices, Nature materials 4 (2005) 366–377.
[3] J. Jiang, Y. Li, J. Liu, X. Huang, C. Yuan, X.W.D. Lou, Recent advances in metal oxide-based electrode architecture design for electrochemical energy storage, Advanced Materials 24 (2012) 5166–5180.
[4] N.S. Choi, Z. Chen, S.A. Freunberger, X. Ji, Y.K. Sun, K. Amine, G. Yushin, L.F. Nazar, J. Cho, P.G. Bruce, Challenges Facing Lithium Batteries and Electrical Double-Layer Capacitors, Angewandte Chemie International Edition 51 (2012) 9994–10024.
[5] P. Simon, Y. Gogotsi, Materials for electrochemical capacitors, Nature materials 7 (2008) 845–854.
[6] G. Wang, L. Zhang, J. Zhang, A review of electrode materials for electrochemical supercapacitors, Chemical Society Reviews 41 (2012) 797–828.
[7] S. Bose, T. Kuila, A.K. Mishra, R. Rajasekar, N.H. Kim, J.H. Lee, Carbon-based nanostructured materials and their composites as supercapacitor electrodes, Journal of Materials Chemistry 22 (2012) 767–784.
[8] L.L. Zhang, X. Zhao, Carbon-based materials as supercapacitor electrodes, Chemical Society Reviews 38 (2009) 2520–2531.
[9] M. Winter, R.J. Brodd, What Are Batteries, Fuel Cells, and Supercapacitors? (Chem. Rev. 2003, 104, 4245-4269. Published on the Web 09/28/2004.), Chemical Reviews 105 (2005) 1021–1021.
[10] J.-M. Tarascon, M. Armand, Issues and challenges facing rechargeable lithium batteries, Nature 414 (2001) 359–367.
[11] R.B. Rakhi, W. Chen, D. Cha, H. Alshareef, Nanostructured Ternary Electrodes for Energy-Storage Applications, Advanced Energy Materials 2 (2012) 381–389.
[12] P. Simon, Y. Gogotsi, Capacitive energy storage in nanostructured carbon–electrolyte systems, Accounts of chemical research 46 (2012) 1094–1103.
[13] L. Hao, X. Li, L. Zhi, Carbonaceous electrode materials for supercapacitors, Advanced Materials 25 (2013) 3899–3904.
[14] J.H. Lee, N. Park, B.G. Kim, D.S. Jung, K. Im, J. Hur, J.W. Choi, Restacking-Inhibited 3D Reduced Graphene Oxide for High Performance Supercapacitor Electrodes, ACS Nano 7 (2013) 9366–9374.
[15] J.H. Lee, W.H. Shin, M.-H. Ryou, J.K. Jin, J. Kim, J.W. Choi, Functionalized Graphene for High Performance Lithium Ion Capacitors, ChemSusChem 5 (2012) 2328–2333.
[16] J. Zhu, M. Chen, H. Qu, Z. Luo, S. Wu, H.A. Colorado, S. Wei, Z. Guo, Magnetic field induced capacitance enhancement in graphene and magnetic graphene nanocomposites, Energy & Environmental Science 6 (2013) 194–204.
[17] Z.S. Wu, D.W. Wang, W. Ren, J. Zhao, G. Zhou, F. Li, H.M. Cheng, Anchoring hydrous RuO2 on graphene sheets for high-performance electrochemical capacitors, Advanced Functional Materials 20 (2010) 3595–3602.
[18] Z. Yu, B. Duong, D. Abbitt, J. Thomas, Highly ordered MnO2 nanopillars for enhanced supercapacitor performance, Advanced Materials 25 (2013) 3302–3306.
[19] B. Wang, T. Zhu, H.B. Wu, R. Xu, J.S. Chen, X.W.D. Lou, Porous Co 3 O 4 nanowires derived from long Co (CO 3) 0.5 (OH)· 0.11 H 2 O nanowires with improved supercapacitive properties, Nanoscale 4 (2012) 2145–2149.
[20] G.A. Snook, P. Kao, A.S. Best, Conducting-polymer-based supercapacitor devices and electrodes, Journal of Power Sources 196 (2011) 1–12.
[21] T.-Y. Wei, C.-H. Chen, H.-C. Chien, S.-Y. Lu, C.-C. Hu, A cost-effective supercapacitor material of ultrahigh specific capacitances: spinel nickel cobaltite aerogels from an epoxide-driven sol-gel process, Advanced materials 22 (2010) 347.
[22] Y. Wang, H. Wei, J. Wang, J. Liu, J. Guo, X. Zhang, B.L. Weeks, T.D. Shen, S. Wei, Z. Guo, Electropolymerized polyaniline/manganese iron oxide hybrids with an enhanced color switching response and electrochemical energy storage, Journal of Materials Chemistry A 3 (2015) 20778–20790.
[23] T. Brezesinski, J. Wang, S.H. Tolbert, B. Dunn, Ordered mesoporous [alpha]-MoO3 with iso-oriented nanocrystalline walls for thin-film pseudocapacitors, Nature materials 9 (2010) 146–151.
[24] J. Xiao, S. Yang, Sequential crystallization of sea urchin-like bimetallic (Ni, Co) carbonate hydroxide and its morphology conserved conversion to porous NiCo 2 O 4 spinel for pseudocapacitors, RSC Advances 1 (2011) 588–595.
[25] C. Yuan, B. Gao, L. Shen, S. Yang, L. Hao, X. Lu, F. Zhang, L. Zhang, X. Zhang, Hierarchically structured carbon-based composites: design, synthesis and their application in electrochemical capacitors, Nanoscale 3 (2011) 529–545.
[26] C. Xia, W. Chen, X. Wang, M.N. Hedhili, N. Wei, H.N. Alshareef, Highly Stable Supercapacitors with Conducting Polymer Core-Shell Electrodes for Energy Storage Applications, Advanced Energy Materials 5 (2015).
[27] J.-H. Kim, K. Zhu, Y. Yan, C.L. Perkins, A.J. Frank, Microstructure and pseudocapacitive properties of electrodes constructed of oriented NiO-TiO2 nanotube arrays, Nano letters 10 (2010) 4099–4104.
[28] X.-h. Xia, J.-p. Tu, X.-l. Wang, C.-d. Gu, X.-b. Zhao, Hierarchically porous NiO film grown by chemical bath deposition via a colloidal crystal template as an electrochemical pseudocapacitor material, Journal of Materials Chemistry 21 (2011) 671–679.
[29] S. Guo, J. Liu, S. Qiu, W. Liu, Y. Wang, N. Wu, J. Guo, Z. Guo, Porous ternary TiO2/MnTiO3@C hybrid microspheres as anode materials with enhanced electrochemical performances, Journal of Materials Chemistry A 3 (2015) 23895–23904.
[30] V. Subramanian, H. Zhu, R. Vajtai, P. Ajayan, B. Wei, Hydrothermal synthesis and pseudocapacitance properties of MnO2 nanostructures, The Journal of Physical Chemistry B 109 (2005) 20207–20214.
[31] J. Liu, J. Jiang, C. Cheng, H. Li, J. Zhang, H. Gong, H.J. Fan, Co3O4 Nanowire@MnO2 Ultrathin Nanosheet Core/Shell Arrays: A New Class of High-Performance Pseudocapacitive Materials, Advanced Materials 23 (2011) 2076–2081.
[32] H. Wang, Z. Xu, H. Yi, H. Wei, Z. Guo, X. Wang, One-step preparation of single-crystalline Fe2O3 particles/graphene composite hydrogels as high performance anode materials for supercapacitors, Nano Energy 7 (2014) 86–96.
[33] R.B. Rakhi, W. Chen, D. Cha, H.N. Alshareef, Substrate Dependent Self-Organization of Mesoporous Cobalt Oxide Nanowires with Remarkable Pseudocapacitance, Nano Letters 12 (2012) 2559–2567.
[34] X.-H. Xia, J.-P. Tu, X.-L. Wang, C.-D. Gu, X.-B. Zhao, Mesoporous Co3O4 monolayer hollow-sphere array as electrochemical pseudocapacitor material, Chemical Communications 47 (2011) 5786–5788.
[35] C. Yuan, J. Li, L. Hou, X. Zhang, L. Shen, X.W.D. Lou, Ultrathin mesoporous NiCo2O4 nanosheets supported on Ni foam as advanced electrodes for supercapacitors, Advanced Functional Materials 22 (2012) 4592–4597.
[36] G. Gao, H.B. Wu, S. Ding, L.M. Liu, X.W.D. Lou, Hierarchical NiCo2O4 Nanosheets Grown on Ni Nanofoam as High-Performance Electrodes for Supercapacitors, Small 11 (2015) 804–808.
[37] Q. Wang, X. Wang, B. Liu, G. Yu, X. Hou, D. Chen, G. Shen, NiCo 2 O 4 nanowire arrays supported on Ni foam for high-performance flexible all-solid-state supercapacitors, Journal of Materials Chemistry A 1 (2013) 2468–2473.
[38] G. Zhang, X.W.D. Lou, Controlled growth of NiCo2O4 nanorods and ultrathin nanosheets on carbon nanofibers for high-performance supercapacitors, Scientific reports 3 (2013).
[39] G.Q. Zhang, H.B. Wu, H.E. Hoster, M.B. Chan-Park, X.W.D. Lou, Single-crystalline NiCo 2 O 4 nanoneedle arrays grown on conductive substrates as binder-free electrodes for high-performance supercapacitors, Energy & Environmental Science 5 (2012) 9453–9456.
[40] H. Jiang, J. Ma, C. Li, Hierarchical porous NiCo 2 O 4 nanowires for high-rate supercapacitors, Chemical Communications 48 (2012) 4465–4467.
[41] A. Tavares, M. Cartaxo, M. da Silva Pereira, F. Costa, Electrochemical study of spinel oxide systems with nominal compositions Ni 1- x Cu x Co 2 O 4 and NiCo 2- y Cu y O 4, Journal of Solid State Electrochemistry 5 (2001) 57–67.

[42] J. Liu, Y. Li, X. Huang, G. Li, Z. Li, Layered Double Hydroxide Nano-and Microstructures Grown Directly on Metal Substrates and Their Calcined Products for Application as Li-Ion Battery Electrodes, Advanced Functional Materials 18 (2008) 1448–1458.
[43] M. Tarasevich, B. Efremov, S. Trasatti, Electrodes of conductive metallic oxides, part A, Elsevier, USA, 1982, pp. 227.
[44] X. Wang, X. Han, M. Lim, N. Singh, C.L. Gan, M. Jan, P.S. Lee, Nickel cobalt oxide-single wall carbon nanotube composite material for superior cycling stability and high-performance supercapacitor application, The Journal of Physical Chemistry C 116 (2012) 12448–12454.
[45] X. Liu, S. Shi, Q. Xiong, L. Li, Y. Zhang, H. Tang, C. Gu, X. Wang, J. Tu, Hierarchical NiCo2O4@ NiCo2O4 core/shell nanoflake arrays as high-performance supercapacitor materials, ACS applied materials & interfaces 5 (2013) 8790–8795.
[46] S. Dong, X. Chen, L. Gu, X. Zhou, L. Li, Z. Liu, P. Han, H. Xu, J. Yao, H. Wang, One dimensional MnO 2/titanium nitride nanotube coaxial arrays for high performance electrochemical capacitive energy storage, Energy & Environmental Science 4 (2011) 3502–3508.
[47] G. Cui, L. Gu, A. Thomas, L. Fu, P.A. van Aken, M. Antonietti, J. Maier, A carbon/titanium vanadium nitride composite for lithium storage, ChemPhysChem 11 (2010) 3219–3223.
[48] B. Avasarala, P. Haldar, Electrochemical oxidation behavior of titanium nitride based electrocatalysts under PEM fuel cell conditions, Electrochimica Acta 55 (2010) 9024–9034.
[49] C. Zhu, P. Yang, D. Chao, X. Wang, X. Zhang, S. Chen, B.K. Tay, H. Huang, H. Zhang, W. Mai, All Metal Nitrides Solid-State Asymmetric Supercapacitors, Advanced Materials (2015).
[50] X. Lu, G. Wang, T. Zhai, M. Yu, S. Xie, Y. Ling, C. Liang, Y. Tong, Y. Li, Stabilized TiN nanowire arrays for high-performance and flexible supercapacitors, Nano letters 12 (2012) 5376–5381.
[51] X. Lu, M. Yu, T. Zhai, G. Wang, S. Xie, T. Liu, C. Liang, Y. Tong, Y. Li, High Energy Density Asymmetric Quasi-Solid-State Supercapacitor Based on Porous Vanadium Nitride Nanowire Anode, Nano Letters 13 (2013) 2628–2633.
[52] C. Zhu, P. Yang, D. Chao, X. Wang, X. Zhang, S. Chen, B.K. Tay, H. Huang, H. Zhang, W. Mai, All Metal Nitrides Solid-State Asymmetric Supercapacitors, Advanced Materials 27 (2015) 4566–4571.
[53] M.Q. Snyder, S.A. Trebukhova, B. Ravdel, M.C. Wheeler, J. DiCarlo, C.P. Tripp, W.J. DeSisto, Synthesis and characterization of atomic layer deposited titanium nitride thin films on lithium titanate spinel powder as a lithium-ion battery anode, Journal of Power Sources 165 (2007) 379–385.
[54] A. Kohandehghan, P. Kalisvaart, K. Cui, M. Kupsta, E. Memarzadeh, D. Mitlin, Silicon nanowire lithium-ion battery anodes with ALD deposited TiN coatings demonstrate a major improvement in cycling performance, Journal of Materials Chemistry A 1 (2013) 12850–12861.
[55] E.M. Lotfabad, P. Kalisvaart, A. Kohandehghan, K. Cui, M. Kupsta, B. Farbod, D. Mitlin, Si nanotubes ALD coated with TiO2, TiN or Al2O3 as high performance lithium ion battery anodes, Journal of Materials Chemistry A 2 (2014) 2504–2516.
[56] H.C.M. Knoops, L. Baggetto, E. Langereis, M.C.M. van de Sanden, J.H. Klootwijk, F. Roozeboom, R.A.H. Niessen, P.H.L. Notten, W.M.M. Kessels, Deposition of TiN and TaN by Remote Plasma ALD for Cu and Li Diffusion Barrier Applications, Journal of The Electrochemical Society 155 (2008) G287–G294.
[57] G. Hasegawa, A. Kitada, S. Kawasaki, K. Kanamori, K. Nakanishi, Y. Kobayashi, H. Kageyama, T. Abe, Impact of Electrolyte on Pseudocapacitance and Stability of Porous Titanium Nitride (TiN) Monolithic Electrode, Journal of The Electrochemical Society 162 (2015) A77–A85.
[58] S.M. George, Atomic layer deposition: an overview, Chemical reviews 110 (2009) 111–131.
[59] J. Elam, D. Routkevitch, P. Mardilovich, S. George, Conformal coating on ultrahigh-aspect-ratio nanopores of anodic alumina by atomic layer deposition, Chemistry of Materials 15 (2003) 3507–3517.
[60] X. Chen, H. Zhu, Y.-C. Chen, Y. Shang, A. Cao, L. Hu, G.W. Rubloff, MWCNT/V2O5 core/shell sponge for high areal capacity and power density Li-ion cathodes, ACS nano 6 (2012) 7948–7955.
[61] J. Ferguson, A. Weimer, S. George, Atomic layer deposition of ultrathin and conformal Al 2 O 3 films on BN particles, Thin Solid Films 371 (2000) 95–104.
[62] H. Zheng, T. Zhai, M. Yu, S. Xie, C. Liang, W. Zhao, S.C.I. Wang, Z. Zhang, X. Lu, TiO 2@ C core–shell nanowires for high-performance and flexible solid-state supercapacitors, Journal of Materials Chemistry C 1 (2013) 225–229.
[63] M. Kaempgen, C.K. Chan, J. Ma, Y. Cui, G. Gruner, Printable Thin Film Supercapacitors Using Single-Walled Carbon Nanotubes, Nano Letters 9 (2009) 1872–1876.
[64] Y. Xu, Z. Lin, X. Huang, Y. Liu, Y. Huang, X. Duan, Flexible solid-state supercapacitors based on three-dimensional graphene hydrogel films, ACS nano 7 (2013) 4042–4049.
[65] G. Wang, H. Wang, X. Lu, Y. Ling, M. Yu, T. Zhai, Y. Tong, Y. Li, Solid-State Supercapacitor Based on Activated Carbon Cloths Exhibits Excellent Rate Capability, Advanced Materials 26 (2014) 2676–2682.
[66] P. Yang, X. Xiao, Y. Li, Y. Ding, P. Qiang, X. Tan, W. Mai, Z. Lin, W. Wu, T. Li, H. Jin, P. Liu, J. Zhou, C.P. Wong, Z.L. Wang, Hydrogenated ZnO Core–Shell Nanocables for Flexible Supercapacitors and Self-Powered Systems, ACS Nano 7 (2013) 2617–2626.